Small-Scale ASR Between Flow Barriers in a Saline Aquifer

van Ginkel, Marloes; des Tombe, Bas; Olsthoorn-Schad, Theo; Bakker, Mark

Citation (APA)
van Ginkel, M., des Tombe, B., Olsthoorn-Schad, T., & Bakker, M. (2016). Small-Scale ASR Between Flow Barriers in a Saline Aquifer. *Groundwater*, *54*(6), 840-850. https://doi.org/10.1111/gwat.12427

Important note
To cite this publication, please use the final published version (if applicable).
Please check the document version above.

Groundwater

Small–Scale ASR Between Flow Barriers in a Saline Aquifer

by Marloes van Ginkel[1,2], Bas des Tombe[3], Theo Olsthoorn[3,4], and Mark Bakker[3]

Abstract

Regular aquifer storage recovery, ASR, is often not feasible for small-scale storage in brackish or saline aquifers because fresh water floats to the top of the aquifer where it is unrecoverable. Flow barriers that partially penetrate a brackish or saline aquifer prevent a stored volume of fresh water from expanding sideways, thus increasing the recovery efficiency. In this paper, the groundwater flow and mixing is studied during injection, storage, and recovery of fresh water in a brackish or saline aquifer in a flow-tank experiment and by numerical modeling to investigate the effect of density difference, hydraulic conductivity, pumping rate, cyclic operation, and flow barrier settings. Two injection and recovery methods are investigated: constant flux and constant head. Fresh water recovery rates on the order of 65% in the first cycle climbing to as much as 90% in the following cycles were achievable for the studied configurations with constant flux whereas the recovery efficiency was somewhat lower for constant head. The spatial variation in flow velocity over the width of the storage zone influences the recovery efficiency, because it induces leakage of fresh water underneath the barriers during injection and upconing of salt water during recovery.

Introduction

Artificial recharge of fresh water for later recovery and use, known as aquifer storage and recovery (aquifer storage recovery [ASR]; Pyne 2005), is increasingly applied for temporal water storage. ASR in brackish or saline aquifers appears hydrologically feasible as was already shown by Cederstrom (1947). However, the problem with fresh water injected into aquifers containing denser salt water is that the fresh water tends to float upward to the top of the aquifer and spread out over the denser salt water, where it is impossible to recover at a later stage. Several researchers have demonstrated

the negative effect of density-induced buoyancy on the recovery efficiency of ASR (e.g. Esmail and Kimbler 1967; Kumar and Kimbler 1970; Merritt 1986; Ward et al. 2007, 2008, 2009; Bakker 2010), where the recovery efficiency is defined as the ratio between injected and recovered fresh water (e.g. Lowry and Anderson 2006). The negative influence of density-induced buoyancy on the recovery efficiency is most severe for small-scale ASR (e.g., Ward et al. 2007, 2009; Bakker 2010; Van Ginkel et al. 2014).

While most scholars studied the buoyancy phenomenon analytically or numerically, only few of them have looked at solutions to overcome this problem for small-scale ASR. At an ASR site in Marathon, Florida, a trickle flow was maintained during the storage period to counteract buoyancy (Pyne 2005). Maliva et al. (2006) proposed well-design optimizations, such as one-way valves, inflatable packers, or additional partially penetrating wells as a solution. In line with these well optimizations, Zuurbier et al. (2014) tested a skimming technique consisting of multiple partially penetrating wells and reached recovery efficiencies on the order of 60% at a small-scale ASR system. Comparable recovery rates were found in numerical simulations by Van Ginkel et al. (2014), who presented an operational paradigm that combines ASR with salt water extraction from below the fresh water zone. The study of Zuurbier et al. (2015) demonstrated the potential benefits of horizontal wells on the recovery efficiency of ASR in coastal areas by numerical simulation.

[1]Corresponding author: Delft University of Technology, Faculty of Civil Engineering and Geosciences, Water Resources Section, P.O. Box 5048, 2600 GA Delft, the Netherlands; marloes.vanginkel@gmail.com

[2]Royal Haskoning DHV, P.O. Box 8520, 3009 AM Rotterdam, the Netherlands.

[3]Faculty of Civil Engineering and Geosciences, Water Resources Section, Delft University of Technology, P.O. Box 5048, 2600 GA Delft, the Netherlands.

[4]Waternet, P.O. Box 94370, 1090 GJ Amsterdam, the Netherlands.

In one of their recovery approaches, Van Ginkel et al. (2014) showed by a numerical simulation that flow barriers at a limited distance around the ASR well increase the recovery efficiency. Flow barriers are vertical walls constructed of sheet piles, clay, or other types of impermeable material. It was argued that salt water extraction from below the fresh water zone is not required if small-scale ASR in saline aquifers is combined with vertical walls, because the vertical walls obstruct the floating fresh water from flowing sideways (Van Ginkel 2015). Flow barriers have not been applied to the authors' knowledge in practical ASR in saline aquifers to this date. Fresh water can be recovered by a network of drains or shallow or horizontal wells. The vertical walls are similar to flow barriers applied to reduce salt water intrusion in coastal aquifers. Anwar (1983) described how partially penetrating barriers across the flow direction modify the flow field and can increase the yield of fresh groundwater resources in unconfined coastal aquifers. Luyun et al. 2011 performed laboratory-scale experiments and numerical simulations to determine the effects of the location and penetration depth of flow barriers on seawater-intrusion control and Kaleris and Ziogas (2013) showed the protective effect of flow barriers on groundwater extractions near the coast.

The objective of this paper is to investigate the flow dynamics and recovery efficiency of small-scale ASR in saline aquifers when combined with surrounding flow barriers. First, the recovery efficiency is computed for several ASR systems to quantify the effect of combining ASR with flow barriers. Second, a laboratory experiment was carried out to examine the behavior of a fresh water volume injected between flow barriers in a saline aquifer during injection, storage, and recovery. Third, simulations were performed to examine the effect of aquifer properties and flow-barrier settings on the recovery efficiency. It was finally investigated if the recovery efficiency could be increased by a layer of gravel below the storage zone.

Problem Description

Consider ASR between two vertical walls in a vertical cross-section (Figure 1). A Cartesian x,y-coordinate system is adopted with the y-axis pointing vertically upward. The aquifer thickness is H [L], the length of the cross section is $2L$ [L], and vertical flow barriers with a penetration depth D [L] are located a distance $2B$ [L] apart. The aquifer is initially filled with saltwater of density ρ_s [M/L^3]. Uniform recharge P [L/T] is applied between the walls to simulate drains or shallow or horizontal ASR wells on top of the aquifer. The hydraulic conductivity of the aquifer k [L/T] is homogeneous and isotropic. The effective porosity of the aquifer is n [−]. The cross-section is symmetric across the y-axis, so that only the positive x-domain is considered in this paper.

Systems with and without flow barriers were simulated with SEAWAT (Langevin et al. 2008) in the *mfLab* environment. Simulations were performed in brackish
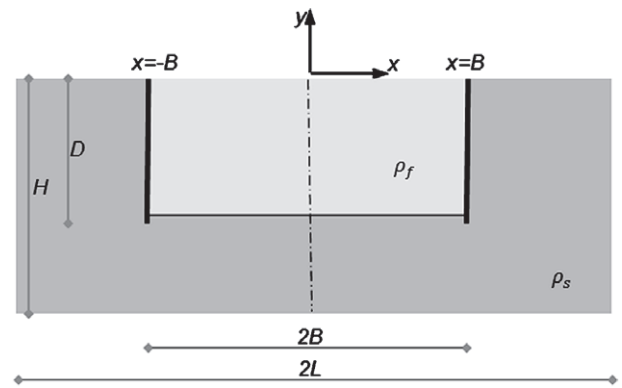

Figure 1. Problem setup: cross-section through an ASR system between two vertical walls.

Table 1
Geometry and Aquifer Data

Parameter	Value
H: Aquifer thickness (m)	30
D: Depth of the barrier (m)	15
L: Length of the model (m)	250
B: Width of the barrier (m)	30
ρ_f: Density fresh water (kg/m^3)	1000
ρ_s: Density salt water (kg/m^3)	1005 and 1025
k: Hydraulic conductivity (m/d)	10
n: Porosity (−)	0.35
P: Recharge (mm/d)	9 and 35
Δx, Δy: Grid size (m)	0.2
α_L: Longitudinal dispersivity (m)	0.1
α_T: Transversal dispersivity (m)	0.02
D_d: Molecular diffusion (cm^2/d)	1×10^{-5}

aquifers ($\rho_s = 1005$ kg/m^3, 5000 mg/L total dissolved solids [TDS]) and saline aquifers ($\rho_s = 1025$ kg/m^3, 42,000 mg/L TDS). The geometry and aquifer data are given in Table 1. Boundary conditions are an impermeable top boundary for $x > B$, a constant head of 0 m at $x = L$, different boundary conditions along the top of the storage zone during ASR operation, as discussed in the next paragraph, and no flow along all other boundaries. Elastic storage was neglected. The total variation diminishing (TVD) scheme was used to solve the solute-transport equation.

The ASR process was repeated for five cycles. The duration of a cycle was one calendar year. One cycle was divided into four periods: an injection period of 3 months with a constant injection rate P along the top of the storage zone, a storage period of 3 months, a recovery period with a constant recovery rate P along the top of the storage zone until the average extracted concentration reached the international drinking water standard of 500 mg/L TDS (maximum 3 months), and an idle period until the year was complete. Simulations were performed for two different injection and recovery rates of $P = 9$ mm/d and $P = 35$ mm/d.
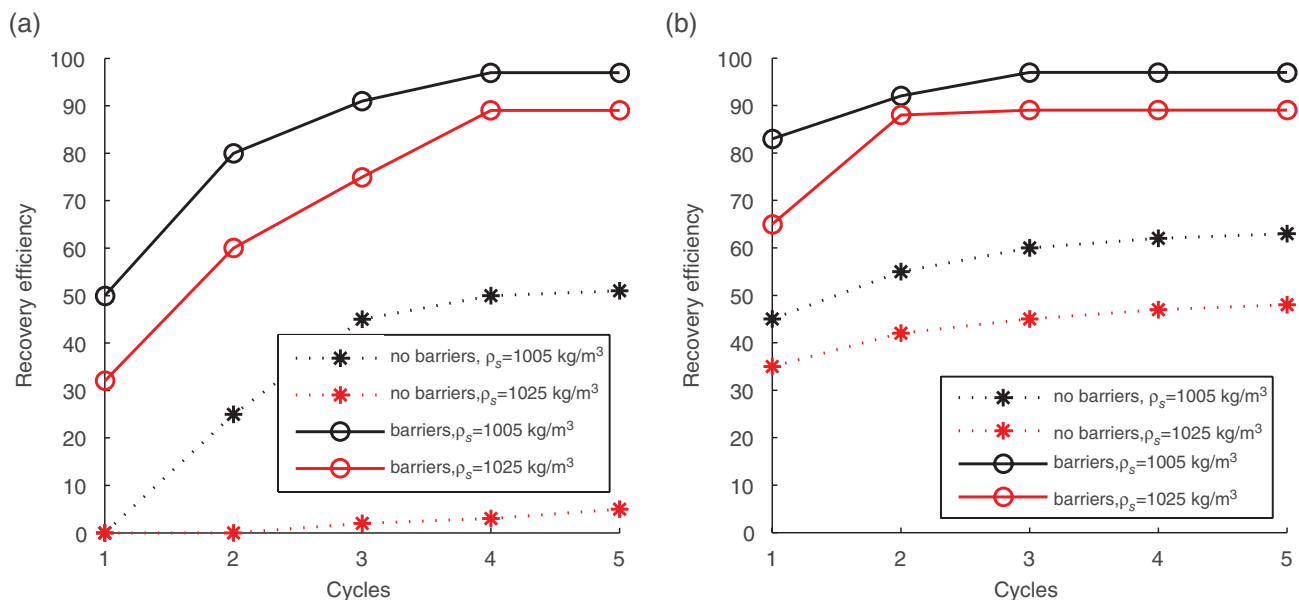
Figure 2. Calculated recovery efficiency in successive cycles for regular ASR and ASR combined with flow barriers: (a) $P = 9$ mm/d; (b) $P = 35$ mm/d. Black lines are brackish aquifers ($\rho_s = 1005$ kg/m^3) and red lines are saline aquifers ($\rho_s = 1025$ kg/m^3).

Results for the recovery efficiency for $P = 9$ mm/d are shown in Figure 2a. The computed recovery efficiency in the first cycle from a brackish aquifer was 50% and from a saline aquifer 35% for the cases with barriers compared with zero for the cases without barriers. The recovery efficiency increased in subsequent cycles, till 97% in the fifth cycle in a brackish aquifer and 89% in a saline aquifer for the cases with barriers compared with 50% in a brackish aquifer and 5% in a saline aquifer for the cases without barriers. The increase in recovery efficiency in successive cycles is consistent with earlier ASR studies (e.g., Kumar and Kimbler 1970; Merritt 1986; Pyne 2005; Ward et al. 2007; Bakker 2010).

Results for $P = 35$ mm/d are shown in Figure 2b. The recovery efficiency without barriers is 45% in a brackish aquifer and 35% in a saline aquifer in the first cycle for this larger injection and recovery rate. The recovery efficiencies for the cases with flow barriers are doubled those of the cases without flow barriers. Fresh water reached the bottom of the flow barriers in the third cycle and fresh water escaped underneath the barriers in subsequent cycles, which made this water unrecoverable so that the recovery efficiency did not increase beyond cycle 4.

The examples in Figure 2 show that the flow barriers lead to significantly improved recovery efficiencies for small-scale ASR systems. In these examples, one set of values was used for the hydraulic conductivity and thickness of the aquifer, width and depth of the flow barriers, and pumping rate. To investigate the flow dynamics further, a laboratory experiment was performed and numerical simulations were conducted to study the effect of density difference, hydraulic conductivity and thickness of the aquifer, width and depth of the flow barriers, and pumping rate.

Physical Model Setup

Physical models are important tools to gain information about fresh and salt water interaction and flow dynamics (e.g., Pennink 1915; Luyun et al. 2011; Stoeckl and Houben 2012). A physical experiment was conducted for the right half of the symmetric flow system (Des Tombe et al. 2011). The experimental setup consisted of an acrylic box of $L = 100$ cm, $H = 17$ cm, and 10 cm width (Figure 3). The main section of the box was packed with glass beads with a diameter of 400-600 μm. The hydraulic conductivity of the glass beads was measured with a Darcy experiment. The hydraulic conductivity was 220 m/d and the porosity was 0.38. An acrylic screen of $D = 12$ cm at $B = 35$ cm functioned as a flow barrier. A salt water reservoir at the right-hand boundary of the box was separated from the main section by a screen with an opening of 1 cm above the box's bottom. The head in the salt water reservoir was maintained at 1 cm above the glass beads bed by a peristaltic inlet/outlet pump in the salt water reservoir.

Tap water was used as fresh water and was dyed with a yellow fluorescent tracer (fluorescein sodium salt) at a concentration of 8 mg/L to visualize the different water types. UV illumination was used to improve the contrast. It was assumed that the effect of the tracer on the viscosity of the fluid was negligible. Table salt at a concentration of 100 g/L was dissolved in tap water to prepare salt water. Water density was measured with a hydrometer. Fresh water density was $\rho_f = 1004$ kg/m^3 and salt water $\rho_s = 1075$ kg/m^3. The box was initially filled with salt water via tubes at the bottom of the box. Beads were packed in layers under completely saturated conditions to prevent air entrapment and were compressed after each layer was placed, similar to Luyun et al. (2011).
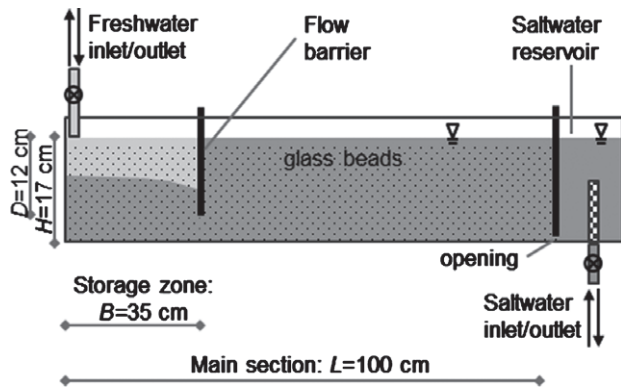
Figure 3. Schematic representation of the experimental setup.

Experimental Results

Fresh water was injected by an inlet pump at 1 cm above the glass beads bed in the upper left-hand corner of the storage zone at a rate of 15 mL/min to establish a fresh water injection layer across the top of the storage zone. Injection stopped as soon as fluorescent tracer started to flow underneath the vertical wall. This occurred after 75 min. The experimental results are shown in Figure 4 which depicts the water in the storage zone between the left part of the experimental setup (corresponding to the center of the storage zone in Figure 3) and the barrier on the right. The bottom of the fresh water zone rotated in the direction of the bottom of the flow barrier during injection (Figure 4a). The inlet pump caused the washout of some glass beads in the upper left-hand corner of the storage zone, which resulted in the dark green color in the upper left-hand corner of the figures. The injection period was followed by a storage period in which no water was injected or extracted. The fresh water zone rotated to a horizontal position in 1240 min. The results at the end of the storage period are shown in Figure 4b.

After the storage period, fresh water was recovered by the outlet pump in the upper left-hand corner of the storage zone at a rate of 15 mL/min. Recovery stopped as soon as the extracted fresh water concentration exceeded the Dutch drinking water standard of 150 mg/L. This occurred after 48 min, resulting in a recovery efficiency of 64%. Figure 4c shows the position of the fresh water zone after 30 min recovery. The fresh water zone rotated in the direction of the top of the flow barrier (Figure 4c). The inclined position of the bottom of the fresh water zone caused salt water upconing along the flow barrier before all fresh water was recovered from the storage zone.

Uranine becomes brighter green in lower concentrations providing an indication of the thickness of the mixing zone between fresh and saline water, highlighted by the dashed white lines in Figure 4. It is noted that uranine has a light sensitivity and that UV illumination may have led to a decrease in concentration during the experiment; its extent was not assessed. The thickness of the mixing zone changed during the experiment (Figure 4). A noticeable feature of the results in Figure 4 is the widening
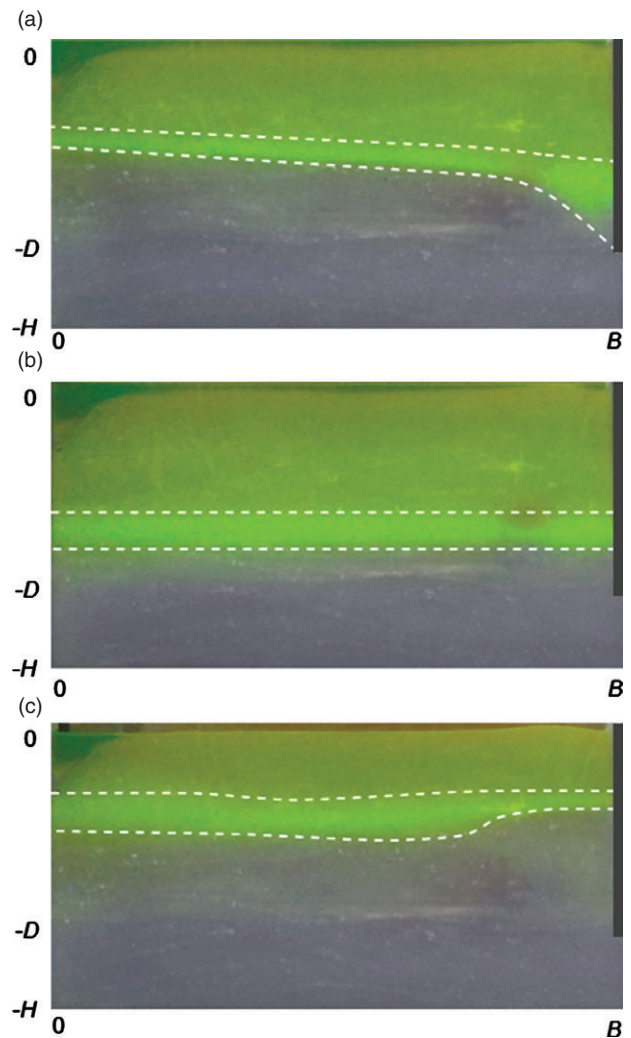

Figure 4. Fresh water zone (green) in the storage zone (between $x = 0$ and $x = B$): (a) end of injection (75 min); (b) end of storage (1315 min); (c) during recovery (1345 min). The dashed white lines indicate the thickness of the mixing zone between fresh water and salt water.

of the mixing zone in the vicinity of the flow barrier during injection and the narrowing of the mixing zone at the same location during recovery.

The experimental results illustrate that the shape of the fresh water zone and the thickness of the mixing zone are influenced by the spatial variation of the flow rate in the storage zone. A large inclination of the bottom of the fresh water zone may result in leakage of fresh water under the flow barrier during injection, before the total storage capacity is reached, or salt water upconing during recovery, before all fresh water is recovered, both decreasing the recovery efficiency.

Comparison Between the Physical and Numerical Model

The physical experiment (Figure 3) was simulated with SEAWAT. The discretization was $\Delta x = \Delta y = 1$ cm. Boundary conditions are an impermeable top boundary

NGWA.org

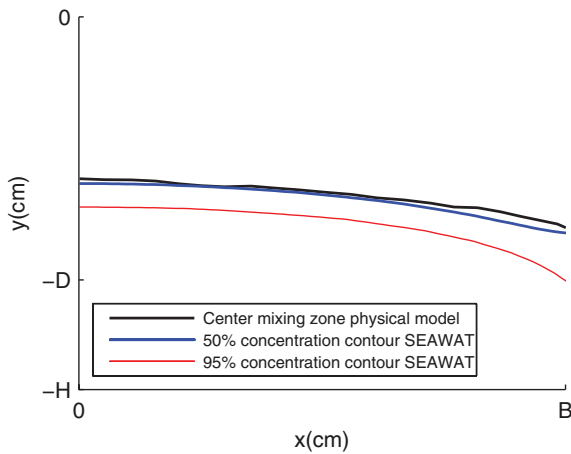M. van Ginkel et al. Groundwater 54, no. 6: 840–850   843

Figure 5. Estimated interface position of the physical model, the 50% concentration contour line and the 95% concentration contour line of SEAWAT at the end of the injection period.

for $x > B$, a constant head of 1 cm at $(x, y) = (L, -H)$, different boundary conditions along the top of the storage zone, and no flow along all other boundaries. Longitudinal and transversal dispersivity were set to 0.1 and 0.01 cm, respectively, and molecular diffusion was 1×10^{-5} cm²/d. A uniform fresh water flux at a rate of 15 mL/min was applied along the top of the storage zone during injection.

The interface position in the storage zone at the end of the injection period is shown in Figure 5. The black curve indicates the center of the mixing zone between fresh water and salt water of the physical model. The blue line is the 50% concentration contour line of SEAWAT. The SEAWAT results are in good agreement with those of the physical model. The red line is the 95% concentration contour as calculated by SEAWAT. This contour passed the bottom of the flow barrier at 75 min, similar to the first leakage of fluorescent tracer under the barrier as was observed in the experiment.

The impermeable top boundary for $x > B$ in the numerical model was slightly different from the physical model boundary condition, where a fixed head was maintained at 1 cm above the glass beads bed. Figure S1, Supporting Information shows that there is no significant difference between the streamline patterns inside the storage zone for a fixed head boundary condition along the top for $x > B$ (red lines) or an impermeable top boundary (blue lines).

Flow Analysis

SEAWAT was used to further investigate the flow and movement of the interface. The interface was defined as the 50% concentration contour line of SEAWAT and dispersion was excluded from the simulations by setting dispersivity and molecular diffusion to zero. Geometry and aquifer data are given in Table 2. The last column of Table 2 presents the range of aquifer parameters used for the sensitivity analysis.

Table 2
Geometry and Aquifer Data

Parameter	Base Value	Range
H: Aquifer thickness (m)	30	—
D: Depth of the barrier (m)	15	—
L: Length of the model (m)	250	—
B: Width of the barrier (m)	30	—
ρ_f: Density freshwater (kg/m³)	1000	—
ρ_s: Density saltwater (kg/m³)	1025	1005–1025
k: Hydraulic conductivity (m/d)	10	1–20
n: Porosity (−)	0.35	—
P: Recharge (mm/d)	35	17–70
$\Delta x, \Delta y$: Grid size (m)	0.2	—
α_L: Longitudinal dispersivity (m)	0	—
α_T: Transversal dispersivity (m)	0	—
D_d: Molecular diffusion (cm²/d)	0	—

The relationship between the specific discharge and the stream function for a divergent-free flow is defined by the well-known relationships (e.g., Bear 1972):

$$q_x = -\frac{\partial \Psi}{\partial y} \qquad (1)$$

$$q_y = +\frac{\partial \Psi}{\partial x} \qquad (2)$$

where Ψ is the stream function [L/T²], x, y are spatial coordinates, and q_x and q_y are the components of the specific discharge vector. De Josselin De Jong (1960) showed that the stream function is a single-valued and continuous function irrespective of the fluids involved. The stream function provides insight in the instantaneous flow field (snapshot in time) by means of its contours, the streamlines. The stream function is constant along a streamline and the difference in stream function values of two streamlines corresponds to the instantaneous discharge between these two streamlines in the cross-section.

The streamlines during the injection of fresh water in a saline aquifer are shown in Figure 6a. The streamlines bend from the initial vertical position to horizontal below the flow barrier. The intensity of the discharge is highest at the bottom of the flow barrier where the streamlines are closest together. No flow occurs in the stagnation point at $(x, y) = (0, -H)$. The black curve indicates the position of the injection front at the end of the injection period. The injection front is inclined due to the higher flow velocity along the barrier compared with the center of the storage zone.

If there is a density difference on either side of the injection front, a jump exists in the specific discharge component parallel to the interface, q_s (e.g., Bear 1972). This discontinuity in q_s along the interface represents a shear flow s that equals the difference between the tangential components of the specific discharge vector
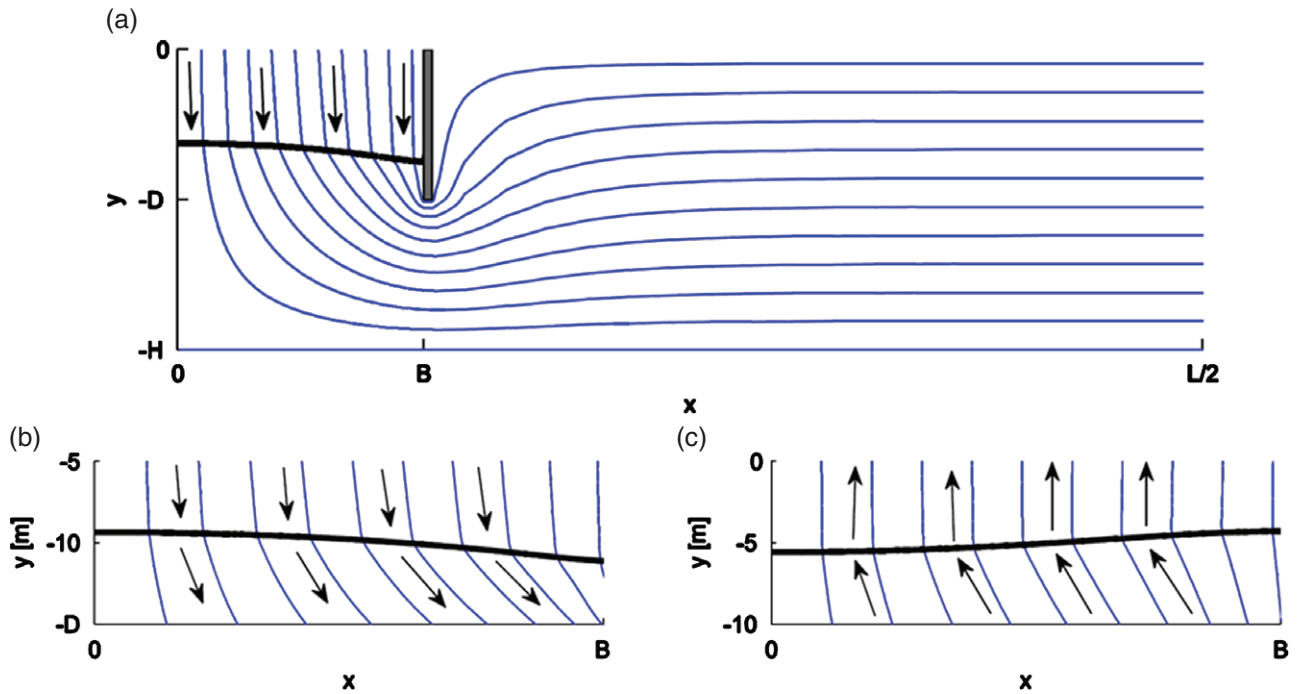
Figure 6. Streamlines ($\Delta\psi = 0.10\,\text{m}^2/\text{d}$) (a) during injection of fresh water in a saline aquifer (note that the horizontal axis only runs to $x = L/2$), (b) detail of injection, and (c) detail of recovery. The black curve represents the position of the interface and the black arrows indicate the flow direction.

across the interface (e.g., Bear 1972):

$$s = q_{t,s} - q_{t,f} = k\frac{\rho_s - \rho_f}{\rho_f}\sin\alpha \qquad (3)$$

where $q_{t,s}$ and $q_{t,f}$ are the components of the specific discharge vector tangential to the interface below and above the interface respectively, and α is the angle between the tangent to the interface and the positive x-axis. A shear flow always exists along an inclined interface that separates two fluids of different density. The component of the specific discharge normal to the interface, q_n, is continuous. The shear flow results in a change in direction and length of the specific discharge vector.

The discontinuous component of the specific discharge at the interface results in a kink in the streamlines at the interface. The kink in the streamlines is shown in the detailed representations of Figure 6b and 6c that present the streamlines near the interface during injection and recovery, respectively. The shear flow increases with increasing slope of the interface (Equation 3). Because the magnitude of the slope increases in x-direction, the refraction of the streamlines at the interface is more pronounced for larger x (Figure 6).

The interface rotates to the stable position during the storage period. The black curve in Figure 7 indicates the position of the interface at the beginning of the storage period and the red line is the interface position at the end of the storage period. All flow during this period is caused by the density difference between the injected and native groundwater.
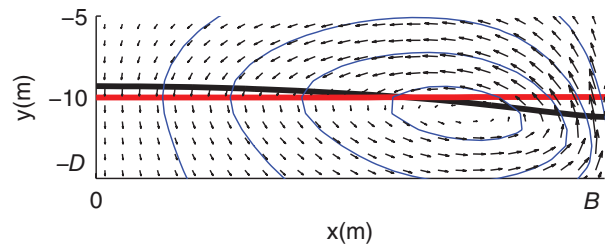

Figure 7. Streamlines (blue lines where $\Delta\psi = 0.02\,\text{m}^2/\text{d}$) and flow vectors at the beginning of the storage period. The black curve represents the position of the interface at the beginning and the red line at the end of the storage period.

Influence of Aquifer Properties and Pumping Rate

The effect of the density difference on the inclination of the interface is shown in Figure 8a. The black lines represent the position of the interface during injection at monthly time intervals in a saline aquifer with $\rho_s = 1025\,\text{kg/m}^3$ and the red lines represent the same in a brackish aquifer with $\rho_s = 1005\,\text{kg/m}^3$. A higher density difference between injected and native groundwater results in a less steep interface position. The shear flow is directly proportional to the density difference (Equation 3) so that a larger density difference helps to flatten the interface.

The effect of different hydraulic conductivities is shown in Figure 8b where the black lines present the results for an aquifer with $k = 1\,\text{m/d}$ and the red lines for $k = 20\,\text{m/d}$. The shear flow is inversely proportional

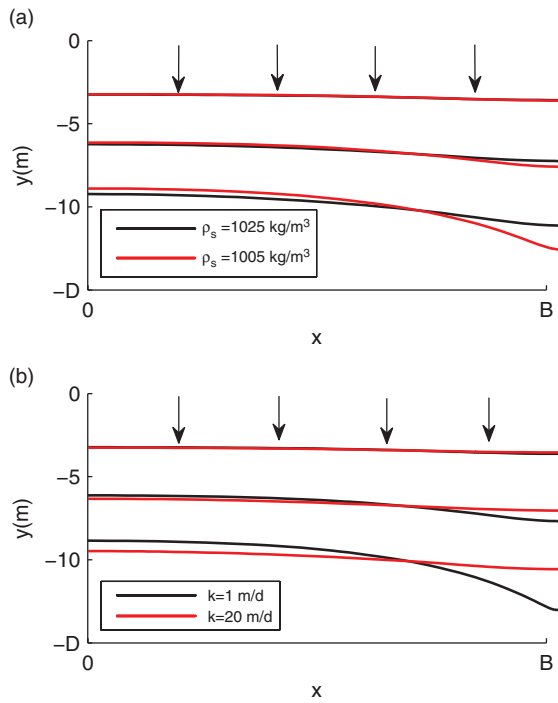M. van Ginkel et al. Groundwater 54, no. 6: 840–850

(a)

(b)

Figure 8. Interface position in the storage zone during injection at monthly intervals, comparison between (a) saline ($\rho_s = 1025\,\text{kg/m}^3$) and brackish aquifer ($\rho_s = 1005\,\text{kg/m}^3$) with $k = 10\,\text{m/d}$ and (b) aquifers with hydraulic conductivity values of 1 and 20 m/d, and $\rho_s = 1025\,\text{kg/m}^3$.

to the hydraulic conductivity (Equation 3) so that higher conductivity values also flatten the interface, as is shown in Figure 8b. The same arguments apply to upconing during recovery, it being more severe when conductivities are smaller and when the salinity difference between the fluids is smaller.

The position of the interface between fresh water and salt water is also influenced by the pumping capacity. The black lines in Figure 9 present the position of the interface at 33%, 66%, and 100% of injected volume for an injection rate of 70 mm/d and the red lines for 17 mm/d. The injection period was adjusted so that the total injected volume was similar in both cases. The inclination of the interface is higher for a larger injection rate. This is always the case when the density of the injection water is smaller than the density of the native groundwater.

Mixing

Eeman et al. (2011) showed that changes in fluid motion over time are important in the development of a fresh water lens and in the development of a mixing zone between this lens and upwelling saline water. This also applies to a fresh water volume between flow barriers in a saline aquifer. To simulate this behavior, similar geometry and aquifer data were used as for the base case (Table 2), but longitudinal and transversal dispersivity were set to 0.1 and 0.01 m, respectively, and molecular diffusion was set to $1 \times 10^{-5}\,\text{cm}^2/\text{d}$. Snapshots from the simulation are shown in Figure 10 for the first ASR-cycle.
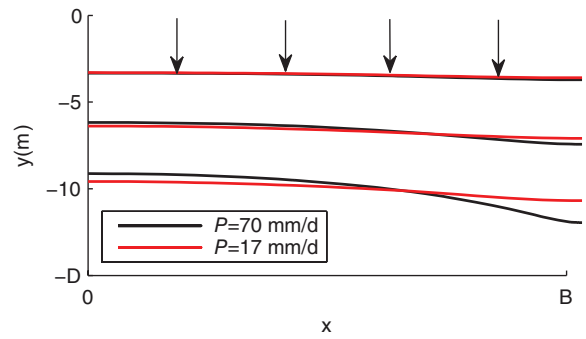

Figure 9. Interface position in the storage zone during injection of 33%, 66%, 100% of injection volume for two injection rates and $\rho_s = 1025\,\text{kg/m}^3$ and $k = 10\,\text{m/d}$.

The width of the mixing zone is defined as the distance between the 95% concentration contours indicated by the pink lines in Figure 10. The mixing zone widens in the vicinity of the flow barrier during injection because the velocity increases in negative y-direction. During recovery, the velocity decreases in upward direction thus narrowing the mixing zone at the same x-location. This was also observed during the experiments (Figure 4).

Flow Barrier Settings

A larger distance between the flow barriers and a larger depth of the flow barriers increases the storage capacity, at least in theory. However, flow rates near and below the flow barrier are larger for a larger distance between the barriers, while the flow velocity in the center stays the same. As a result, the inclination of the interface near the toe of the flow barrier increases for increasing ratios of the distance between the barriers and the depth of the barrier. Similarly, the flow rates in the opening under the flow barrier increase for increasing ratio between the depth of the barrier and the thickness of the aquifer. Also, leakage of fresh water underneath the barriers during injection occurs earlier for larger B/D and D/H ratios, and the recovery efficiency declines along with it.

The recovery efficiency is shown for five successive cycles for different ratios between the depth D of the barrier and the thickness of the aquifer H, and different ratios between the width B between the flow barriers and D (Figure 11). The highest recovery efficiency (on the order of 95% in the fifth cycle) is obtained for cases where the flow barriers penetrate a quarter of the thickness of the aquifer ($D/H = 0.25$, black lines in Figure 11). Note that all three black lines ($D/H = 0.25$) are on top of each other in Figure 11, as different B/D ratios have no influence on the recovery efficiency for these cases.

For cases with $D/H = 0.5$ (blue lines in Figure 11) the highest recovery efficiency is obtained for flow barriers where $B/D = 1$ and $B/D = 2$. For the case with a B/D ratio of 4, leakage underneath the barrier occurred in the first cycle after 50 days of injection. The recovery efficiency of the first cycle was 55% for this case. Recovery efficiencies increased in subsequent cycles,
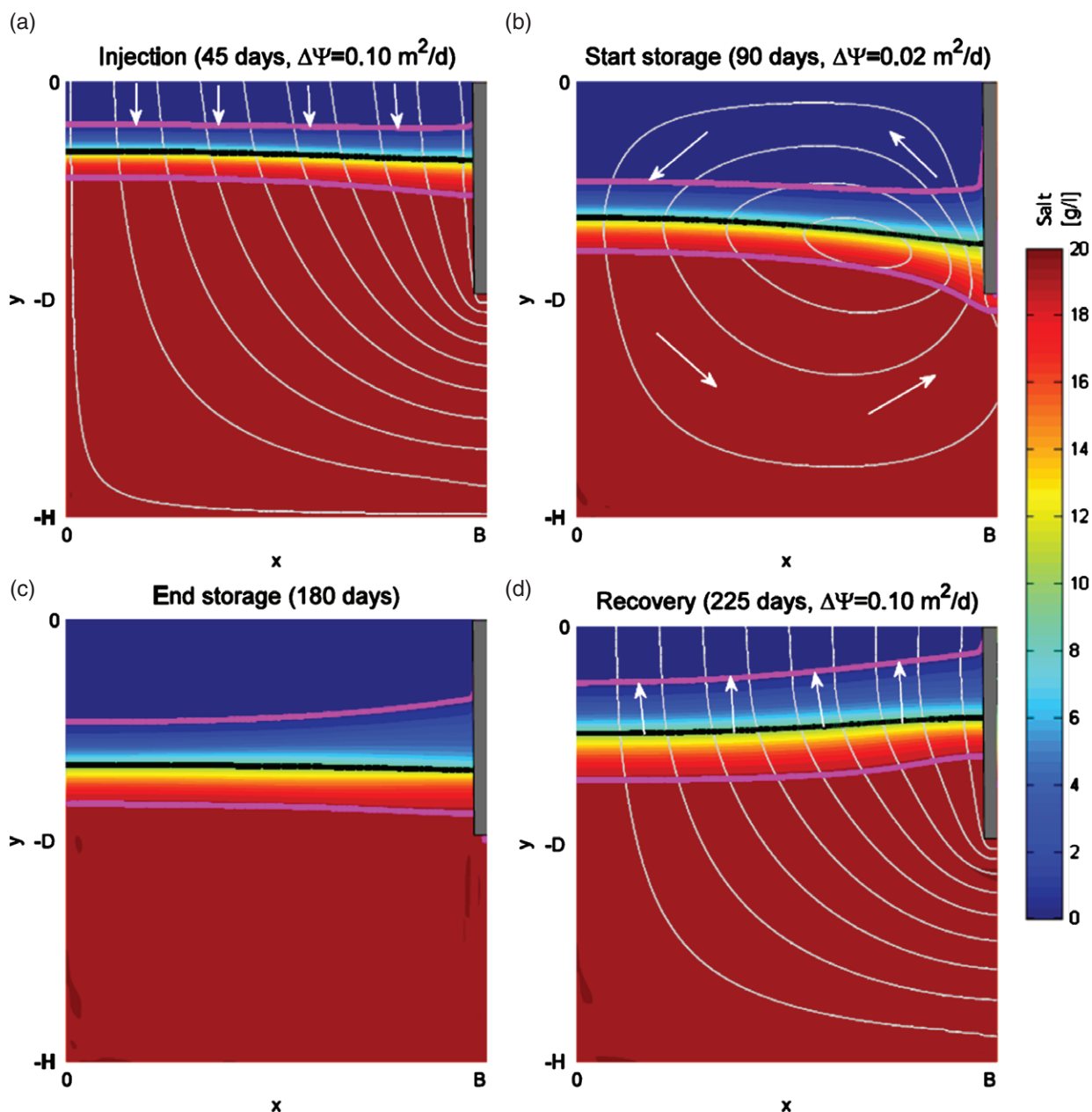
Figure 10. Flow simulation snapshots for (a) injection, (b) start storage, (c) end storage, and (d) recovery. The white lines are streamlines, the black curve is the 50% concentration contour line, and the pink lines are the 95% concentration contour lines.

until 80% in the third cycle, compared with 90% for the cases with a B/D ratio of 1 and 2.

Lowest recovery efficiencies were obtained for cases with D/H ratio $= 0.25$ (red lines in Figure 11) in combination with a large width between the barriers. Leakage underneath the barrier during injection and upconing along the barrier during recovery resulted in a recovery efficiency of 40% in the first cycle, until 70% in the fifth cycle for this case.

Leakage Through the Walls

Leakage through the flow barriers may occur due to construction errors, cracks caused by uneven settlement,

and desiccation of clays. The larger head in the fresh water storage zone compared with the surrounding saline aquifer forces outward leakage during injection and storage. This is illustrated in Figure S2 that shows snapshots for the simulation with an opening in the flow barrier at $y = -5$ m of 0.2 m height. The 500 mg/L contour line reached the opening after 60 days of injection. The outward flow of fresh water continued during the storage period until the head difference on both sides of the flow barrier became equal. Inflow of saline water occurred during recovery, when the head in the storage zone was low. The recovery efficiency was 55%, a loss of 10% compared with the 65% without an opening in the flow barrier.
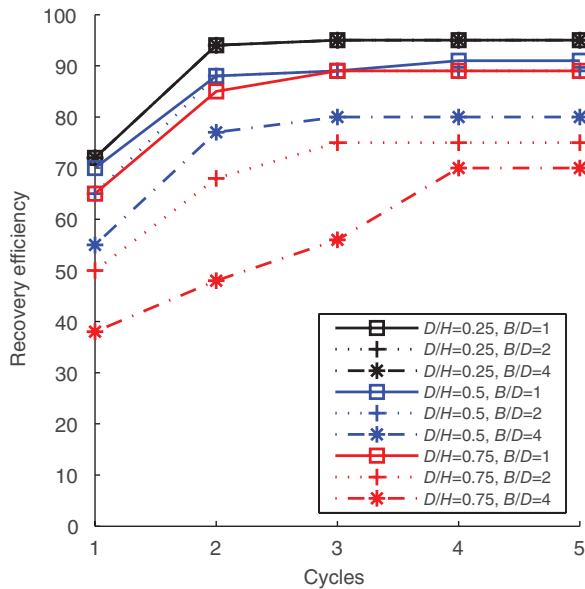
Figure 11. Calculated recovery efficiency in successive cycles for different flow barrier settings; width B between flow barriers, thickness H of the aquifer, and depth D of the barriers.

Gravel Layer below the Storage Zone

The storage capacity can be increased by a layer of gravel below the storage zone. The high hydraulic conductivity of the gravel layer ensures relatively uniform head gradients in the storage zone, resulting in almost vertical flow, and reduction of the inclination of the interface. The construction of gravel layers may be feasible when constructing artificial aquifers such as in man-made islands. A storage zone with a gravel layer at the depth of the barriers was simulated. The results are shown in Figure S3. A layer of gravel of 1 m height with a hydraulic conductivity of 1000 m/d was located between $y = D = -15$ and -16 m. The recovery efficiency of this simulation is 75%, 10% more than 65% efficiency without a gravel layer. This simulation was also performed for a layer of coarse sand with a hydraulic conductivity of 100 m/d resulting in a slightly lower recovery efficiency of 72%.

Injection by a Constant Head in the Storage Zone

So far, injection and recovery were simulated as uniform fluxes along the top of the storage zone. In practice, injection, and recovery may be realized by a head difference between the storage zone and the aquifer. Consider an unconfined aquifer with geometry and aquifer data as presented in Table 2 with an initial head of 0 m and a constant head boundary of 0 m at $L = 2000$ m. Storage changes are included in this simulation; the specific storage coefficient is 1e-5 m^{-1} and the phreatic storage coefficient is 0.20. The head in the storage zone is raised to a constant head of 1.4 m and kept constant for an injection period of 3 months.

The phreatic surface during injection is shown in Figure 12a. The phreatic surface just outside the flow barrier is lower than the phreatic surface inside the storage zone due to the head loss of water flowing around the flow barrier. The fresh water head at the bottom of the flow barrier decreases through time, even though the phreatic surface inside the storage zone is fixed at 1.4 m. This is caused by the increase of fresh water, which is lighter than salt water.

If the storage zone is deep enough, fresh water injection with a fixed head will come to a halt in accordance with the Badon Ghijben Herzberg relation, which states that the maximum depth of the fresh water floating on top of saline water is equal to $y = h\rho_f/(\rho_s - \rho_f)$, where h is the phreatic surface in the storage zone above the water level in the surrounding saline aquifer. For $h = 1.4$ m, $\rho_f = 1000$ kg/m^3, and $\rho_s = 1025$ kg/m^3, the maximum depth of the fresh water zone is $y = -56$ m, provided that the walls are that deep.

The injection period is followed by a storage period of 3 months without prescribed head in the storage zone. The phreatic surface recedes towards the initial value, but the storage period is too short to allow the phreatic surface to drop to 0 m. At the end of the storage period, the phreatic surface in the storage zone is 0.8 m (Figure 12b). The storage period is followed by a recovery period of 3 months in which the head in the storage zone is kept constant at -1 m. The phreatic surface during recovery is shown in Figure 12c.

The volume of injected water in the storage zone under fixed-head conditions is compared with the volume under a constant and uniform injection/recovery rate (Figure 13). For the fixed-head case, the injection rate is larger at the beginning of the injection period than at the end, but the total injection volume is similar to the case of constant, uniform injection. Similarly, recovery is much larger at the beginning of the recovery period. This could be modified by lowering the water level in the storage zone gradually during recovery.

The recovery efficiency for the first cycle under fixed-head conditions is 48% compared with 65% under a constant and uniform injection/recovery rate. One of the reasons that the recovery efficiency under fixed-head conditions is lower is that the relatively high recovery rate at the beginning of the recovery period results in quicker upconing of salt water along the flow barrier. Furthermore, the head in the storage zone is 1 m lower during recovery and the 500 mg/L concentration contour, therefore, reaches the recovery drains sooner.

Conclusions

The recovery efficiency was investigated of small-scale ASR systems in brackish and saline aquifers in combination with flow barriers. Recovery efficiencies of small-scale ASR systems are generally so low that ASR is not a solution. The use of barriers increases the recovery efficiencies to acceptable levels for the cases investigated. Fresh water recoveries on the order of 65%
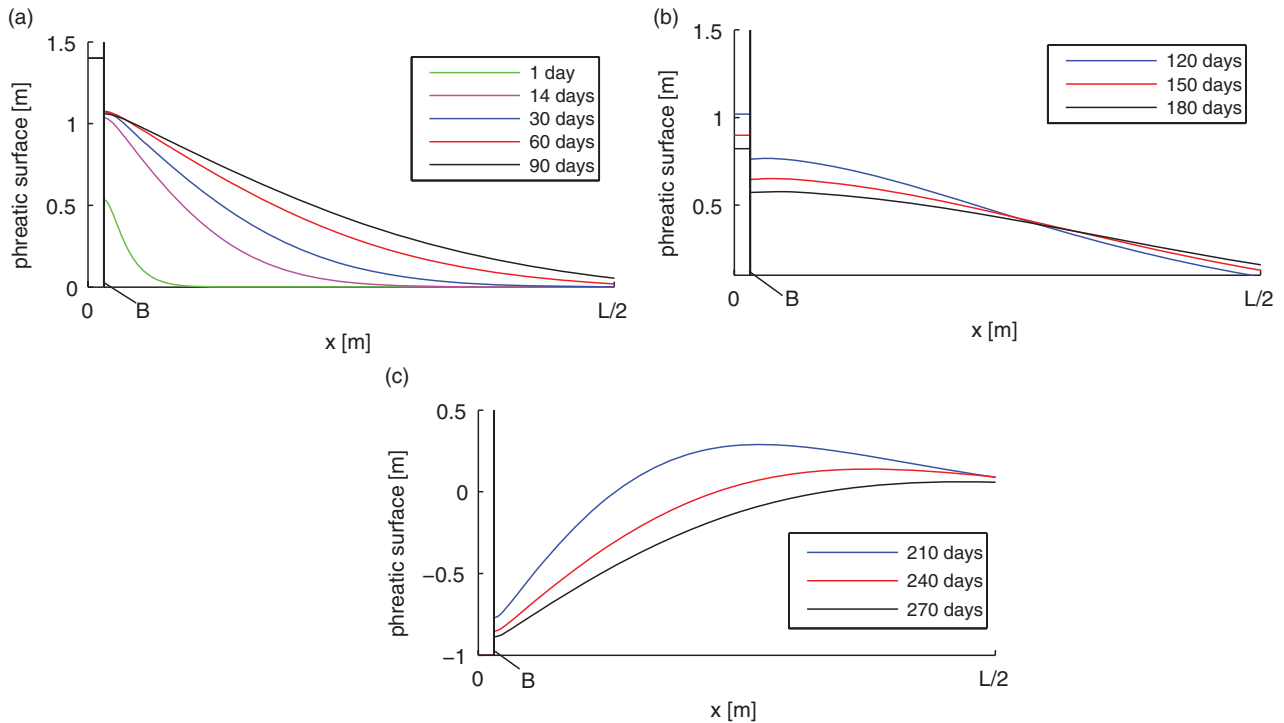
Figure 12. Phreatic surface during (a) injection, (b) storage, and (c) recovery for prescribed heads in the storage zone. Note that the horizontal axis only runs to $x = L/2$.
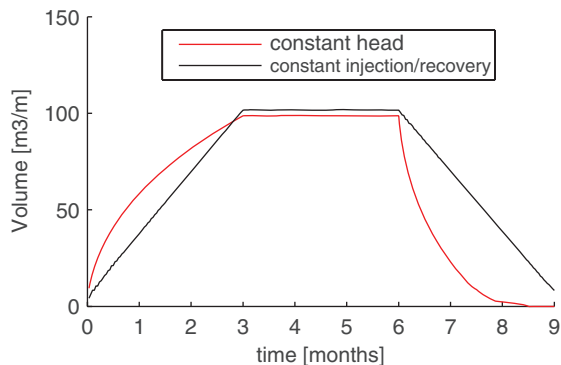

Figure 13. Injected water in the storage zone in one ASR cycle for constant heads and constant injection/recovery rates.

in the first cycle and up to 90% in the following cycles were achieved for the studied configurations with constant flux whereas the recovery efficiency is somewhat lower for constant head.

The shear flow along the interface is proportional to the density difference between injected and native groundwater so that larger density differences reduce the inclination of the interface and increase the fresh water storage capacity. The shear flow is inversely proportional to the hydraulic conductivity so that higher conductivity values also flatten the interface. The inclination of the interface is smaller for lower pumping rates. The recovery efficiency declines for increasing ratio between the width and depth of the flow barriers and for increasing ratio between the depth of the flow barriers and the thickness of

the aquifer. Leakage through gaps in the enclosing walls reduces the recovery efficiency. A gravel layer at the bottom of the storage zone, which may be added to man-made islands, results in more uniform vertical head gradients in the storage zone, which enhances the recovery efficiency.

Supporting Information

Additional Supporting Information may be found in the online version of this article:

Figure S1. Streamlines ($\Delta\psi = 0.10 \, \text{m}^2/\text{d}$) during injection of fresh water in a saline aquifer for two cases. The black curve is the 50% concentration contour line. Note that the horizontal axis only runs to $x = L/2$.

Figure S2. Flow simulation snapshots for (a) injection, (b) start storage, (c) end of storage, and (d) recovery with an opening in the flow barrier at $y = -5 \, \text{m}$. The white lines are streamlines, the black curve is the 50% concentration contour line and the pink lines are the 95% concentration contour lines.

Figure S3. Flow simulation snapshots with a layer of gravel under the storage zone. The white lines are streamlines, the black curve is the 50% concentration contour line, and the pink lines are the 95% concentration contour lines.

References

Anwar, H.O. 1983. The effect of a subsurface barrier on the conservation of freshwater in coastal aquifers. *Water Resources Research* 17, no. 10: 1257–1265.

NGWA.org

M. van Ginkel et al. Groundwater 54, no. 6: 840–850   849

Bakker, M. 2010. Radial Dupuit interface flow to assess the aquifer storage and recovery potential of saltwater aquifers. *Hydrogeology Journal* 18: 107–115. DOI:10.1007/s10040-009-0508-1.

Bear, J. 1972. *Dynamics of Fluids in Porous Media*. New York: Dover.

Cederstrom, D.J. 1947. *Artificial Recharge of a Brackish Water Well*, 14, 14, 31–73. Richmond, Virginia: Virginia Chamber Commerce.

De Josselin De Jong, G. 1960. Singularity distributions for the analysis of multiple fluid flow through porous media. *Journal of Geophysical Research* 65: 3739–3758.

Des Tombe, B.F., M. van Ginkel, T.N. Olsthoorn. 2011. Aquifer storage recovery, the storage tank method, can the storage tank method increase the recovery efficiency? In *Proceedings Salt Water Intrusion Meeting 22*, Buzios, Brazil., ed. G. Cardoso da Silva Jr & D. Montenegro.

Eeman, S., A. Leijnse, P.A.C. Raats, and S.E.A.T.M. van der Zee. 2011. Analysis of the thickness of a fresh water lens and of the transition zone between this lens and upwelling saline water. *Advances in Water Resources* 34: 291–302. DOI:10.1016/j.advwatres.2010.12.001.

Esmail, O.J., and O.K. Kimbler. 1967. Investigation of the technical feasibility of storing fresh water in saline aquifers. *Water Resources Research* 3, no. 3: 686–695.

Kaleris, V.K., and A.I. Ziogas. 2013. The effect of cutoff walls on saltwater intrusion and groundwater extraction in coastal aquifers. *Journal of Hydrology* 476: 370–383.

Kumar, A., and O.K. Kimbler. 1970. Effect of dispersion, gravitational segregation, and formation stratification on the recovery of freshwater stored in saline aquifers. *Water Resources Research* 6, no. 6: 1689–1700.

Langevin, C.D., D.T. Thorne, Jr., A.M. Dausman, M.C. Sukop, W. Guo. 2008. *SEAWAT Version 4: A Computer Program for Simulation of Multi-Species Solute and Heat Transport*, U.S. Geological Survey Techniques and Methods Book 6, Chapter A22, 39 p.

Lowry, C.S., and M.P. Anderson. 2006. An assessment of aquifer storage recovery using groundwater flow models. *Ground Water* 44, no. 5: 661–667. DOI:10.1111/j.1745-6584.2006.00237.x.

Luyun, R. Jr., K. Momii, and K. Nakagawa. 2011. Effects of recharge wells and flow barriers on seawater intrusion. *Ground Water* 49, no. 2: 239–249. DOI:10.1111/j.1745-6584.2010.00719.x.

Maliva, R.G., W. Guo, and T.M. Missimer. 2006. Aquifer storage and recovery: Recent hydrogeological advances and system performance. *Water Environment Research* 78, no. 13: 2428–2435.

Merritt, M.L. 1986. Recovering fresh water stored in saline limestone aquifers. *Ground Water* 24, no. 4: 516–529.

Pennink, J.M.K. 1915. *Grondwater Stroombanen* (motions of groundwater–results of researches made in the years 1904 and 1905, into the form of lines of flow for sub-soil water motion in pure sand). Amsterdam, the Netherlands: Stadsdrukkery Amsterdam the Netherlands 1915. www.citg.tudelft.nl/index.php?id=19739&L=1.

Pyne, R.D.G. 2005. *Aquifer Storage Recovery: A Guide to Groundwater Recharge Through Wells*, ASR Press 2nd edition (2005), ISBN 0977433706, 608 pp, Gainesville, Florida, USA.

Stoeckl, L., and G. Houben. 2012. Flow dynamics and age stratification of freshwater lenses: Experiments and modeling. *Journal of Hydrology* 458–459: 9–15. DOI:10.1016/j.jhydrol.2012.05.070.

Van Ginkel, M. 2015. Aquifer design for freshwater storage and recovery in artificial islands and coastal expansions. *Hydrogeology Journal* 23: 615–618. DOI:10.1007/s10040-015-1245-2.

Van Ginkel, M., T.N. Olsthoorn, and M. Bakker. 2014. A new operational paradigm for small-scale ASR in saline aquifers. *Ground Water* 52: 685–693. DOI:10.1111/gwat.12113.

Ward, J.D., C.T. Simmons, P.J. Dillon, and P. Pavelic. 2009. Integrated assessment of lateral flow, density effects, and dispersion in aquifer storage and recovery. *Journal of Hydrology* 370: 83–99. DOI:10.1016/j.hydrol.2009.02.055.

Ward, J.D., C.T. Simmons, and P.J. Dillon. 2008. Variable-density modelling of multiple-cycle aquifer storage and recovery (asr): importance of anisotropy and layered heterogeneity in brackish aquifers. *Journal of Hydrology* 356: 93–105. DOI:10.1016/j.jhydrol.2008.04.012.

Ward, J.D., C.T. Simmons, and P.J. Dillon. 2007. A theoretical analysis of mixed convection in aquifer storage and recovery: how important are density effects? *Journal of Hydrology* 343: 169–186. DOI:10.1016/j.jhydrol.2007.06.011.

Zuurbier, K.G., J.W. Kooiman, M.M.A. Groen, B. Maas, and P.J. Stuyfzand. 2015. Enabling successful aquifer storage and recovery of freshwater using horizontal directional drilled wells in coastal aquifers. *Journal of Hydrologic Engineering* 20: 3. DOI:10.1061/(ASCE)HE.1943-5584.0000990.

Zuurbier, K.G., W.J. Zaadnoordijk, and P.J. Stuyfzand. 2014. How multiple partially penetrating wells improve the freshwater recovery of coastal aquifer storage and recovery (ASR) systems: a field and modeling study. *Journal of Hydrology* 509: 430–441. DOI:10.1016/j.jhydrol.2013.11.057.